A Probabilistic Atlas of Human Visual Areas and Information-Theoretic Analysis of Individual Variability in Their Loci

AUTHOR(S):

Yamamoto, Hiroki

CITATION:

Yamamoto, Hiroki. A Probabilistic Atlas of Human Visual Areas and Information-Theoretic Analysis of Individual Variability in Their Loci. Advanced Brain Neuroimaging Topics in Health and Disease - Methods and Applications 2014: 219-244

ISSUE DATE:

2014-05-31

URL:

http://hdl.handle.net/2433/197936

Chapter 9

A Probabilistic Atlas of Human Visual Areas and Information-Theoretic Analysis of Individual Variability in Their Loci

Hiroki Yamamoto

Additional information is available at the end of the chapter

http://dx.doi.org/10.5772/30760

1. Introduction

The human visual cortex consists of multiple functionally distinct visual areas that have been individually localized on the cortical surface by brain imaging of their associated retinotopic activity. Thus, their locations can be quantitatively compared across individuals once they are expressed in a common coordinate space. In several studies (Dougherty et al. 2003, Fischl et al. 1999b, Hasnain et al. 1998), such comparisons have been performed using the Talairach stereotactic coordinate system (Talairach et al. 1967, Talairach & Tournoux 1988) as the common anatomical space. Because the Talairach system has been commonly used as a standard to describe the loci of brain activation or lesions, and to normalize the functional data between individual brains, evaluation of the interindividual variability within the Talairach space is essential for reliably interpreting a broad range of brain function data.

The Talairach system considers interindividual variations in overall brain size and shape but not the variations of smaller scale structures, such as the cortical sulci and gyri, which differ substantially and heterogeneously between individuals (Ono et al. 1990). Consequently, interindividual variability within the Talairach space is not only extensive, but also complex in morphology. Analysis of this variability is therefore not straightforward and requires conceptual and practical simplification.

Recently, we have proposed that inconsistency and uncertainty are fundamental concepts characterizing the interindividual variability within the visual areas (Yamamoto et al. 2011). This inconsistency refers to the disparity between the individuals regarding the location of a particular visual area. The inconsistency in the Talairach space has been assessed in several studies by calculating the variance of the position of a representative point within a visual area

(Dougherty et al. 2003, Hasnain et al. 1998) or by constructing a probabilistic map in which each point is associated with a probability that the visual area resides there (Amunts et al. 2000, Fischl et al. 1999b). Although the inconsistency provides a good basis for analyzing a single, isolated area, it is inherently insufficient for regulating multiple visual areas with pairwise adjacency. When transforming multiple areas together into Talairach space, their adjacency causes overlaps between the neighboring areas of different individuals. Therefore, in evaluating the interindividual variability in multiple visual areas, we must address another variable, uncertainty.

This uncertainty relates to the difficulty of knowing which visual areas reside at a given position where the greater the number of overlaps between the different areas, the greater the degree of uncertainty. We should emphasize that uncertainty is conceptually dissociated from inconsistency. Even if there is no area that has a high probability of being present at an anatomical point, the uncertainty at the point is zero if only a single area has a non-zero probability of being present. Conversely, even if an area has a high probability of being present, the uncertainty is large if other areas also have a high probability of being present. When brain activation is observed at a region described as having a high probability but also has a high uncertainty area, we cannot confidently attribute this region to a specific anatomical and functional area. In addition, when the individual brain activations are pooled in Talairach space, caution is warranted regarding the source of activation at such points because the activations of different areas are probably highly confounded. These considerations suggest that quantification of the uncertainty is crucial for reliable interpretation of the functional data in Talairach space. However, this issue has not been investigated.

In the present study, we applied a probabilistic and information theoretical framework to quantify the uncertainty and the inconsistency of multiple human visual areas that were localized based on functional MRI (fMRI) retinotopy measurements. Inconsistency was estimated by generating a probability map based on 10 hemispheres of five subjects, where each point was associated with a probability that it belonged to each retinotopic area. We used the Shannon entropy (Shannon 1948) as an uncertainty measure and generated a novel map we called an entropy map, where each point is associated with a Shannon entropy computed from the probability that the point belongs to each of the visual areas (Eq. (1) in the section 2.3). Generally, the Shannon entropy serves as a useful measure to quantify the uncertainty of a situation (Cencov 1982). In our study, the relevance is when one wants to predict or judge a visual area at a given Talairach point in clinical practice or scientific research, where higher entropy equates to a higher probability of incorrect classification. Using the probability and entropy maps, we analyzed the inconsistency and uncertainty of the locations of retinotopic areas registered in Talairach space.

Although Talairach registration was originally described as piecewise linear transformations, there are a number of methods used, where these include two main types; namely volume-based methods using linear, piecewise-linear, or nonlinear transformations and surface-based methods, allowing for a more precise alignment of the sulcal and gyral patterns (see Gholipour et al. 2007 for a recent comprehensive review). The choice of the transformation method is an important consideration that influences the results of our analysis. In our recent study

http://dx.doi.org/10.5772/30760

(Yamamoto et al. 2011), we employed a sophisticated surface-based method (Fischl et al. 1999b). In the present study, we used a single linear transformation (nine parameters, three each for translation, rotation, and orthogonal scaling) for the entire brain (Desmond & Lim 1997). Many more sophisticated, methods such as nonlinear volume methods (Ashburner 2007, Woods et al. 1998) and surface-based methods (Drury et al. 1996, Fischl et al. 1999b, Thompson et al. 1997) subsume and therefore outperform this method. Thus, the probability and entropy maps created using a single linear transformation can provide a baseline for the evaluation of the inconsistency and uncertainty in Talairach space. Understanding the limits of the transformation is important for performing reliable group analysis and interpreting the published Talairach coordinates of the activation foci because the linear transformation is still commonly used in both basic and clinical neuroscience.

2. Methods

2.1. Imaging

We studied ten hemispheres from five normal subjects (one female, four males; mean 33 years). The subjects were in good health with no past history of psychiatric or neurological disease. The study protocols were approved by the ethical committees of our institutions. All subjects provided written, informed consent prior to study enrollment. The structural and functional MRI measurements were performed using a standard clinical 1.5 Tesla scanner (GE, Signa NV/i). Prior to the experimental scans, high-contrast T1-weighted three-dimensional (3D) SPGR structural images (echo time (TE) = 3.0 ms, repetition time (TR) = 56 ms, flip angle (FA) = 55°; excitations (NEX) = 1, voxel size (VS) = 0.781 × 0.781 × 1.4 or 0.938 × 0.938 × 1.4 mm) of the whole brain were recorded for each subject, which was used for reconstructing the individual brain surface. For each subject, three types of images were obtained on each scan day, with a standard flexible surface coil placed at the occipital pole. First, T1-weighted Inversion Recovery 3D Fast SPGR structural images (TE = 2.7 ms, TR = 6.0 ms, inversion time (TI) = 600 ms, FA = 15°; NEX = 1, VS = 0.781 × 0.781 × 1.4 mm) were acquired for anatomical registration. Second, a set of 16 (three subjects) or 17 (two subjects) adjacent high-resolution T1-weighted spin echo anatomical slices (TE = 9 ms, TR = 420 ms, NEX = 2, VS = 0.781 × 0.781 × 4 mm) was obtained. Finally, multiple functional scans (6 – 8) were obtained in the same slice positions as the anatomical slices while the subject viewed visual stimuli (e.g., a flickering checkerboard ring), using a T2*-weighted two-dimensional gradient echo, echo planar imaging (TE = 50 ms, TR = 2000 ms, FA = 90°, VS = 1.563 × 1.563 × 4 mm).

2.2. Localization of retinotopic areas

After reconstructing each individual's cortical surface, locations of the retinotopic visual areas were identified with fMRI and standard retinotopic mapping procedures (Table 1). The surface was reconstructed to lie approximately in the middle of the gray matter, using a method that was a hybrid of volume segmentation (Drury et al. 1999) and surface deformation (Dale & Sereno 1993). We used mrGray software (Teo et al. 1997) for volume segmentation and a

custom software for surface generation. The software generated an initial surface at the border of the white and gray matter using a marching cube algorithm (Lorensen & Cline 1987) and then deformed it to lie in the middle of the gray matter using the deformable template algorithm (Dale & Sereno 1993).

Technique	Method	Software
Cortical surface reconstruction	Step 1. Anatomical volume segmentation (cerebrospinal fluid, gray matter, white matter)	mrGray (Teo et al., 1997)
	Step 2. Triangular tessellation with the marching cube algorithm (Lorensen & Clein, 1987)	in-house software called BrainFactory (Yamamoto et al., 2002, 2008, 2011) written in C++ & Tcl/Tk using Visualization Toolkit (Kitware inc.)
	Step 3. Deformation of the tessellated surface with the deformable template algorithm (Dale & Sereno, 1993)	BrainFactory
Localization of retinotopic areas	Phase-encoding mapping with fMRI (Engel et al., 1994) Visual stimuli: a rotating wedge for visual field angular mapping and a expanding (fovea-16 deg eccentricity) annulus for eccentricity mapping, 60s /rotation(expansion) × 6 cycles Parcellation of visual areas: visual inspection of the retinotopy and the visual filed sign maps (Sereno et al., 1995)	BrainFactory
Brain registration	A linear rigid volume-based method (Desmond & Lim, 1997) Parameters: 9 parameters (3 scalings, 3 rotations, 3 translations) determined by visual inspection of anatomical landmarks Target brain:10 hemispheres from 5 subjects	BrainFactory

Table 1. Summary of key techniques

The surface regions delimiting areas V1d, V2d, V3d, V3B, V3A, V7, LOc, MT+, V1v, V2v, V3v, V4v, and V8 were determined by phase-encoded retinotopic mapping methods (DeYoe et al. 1994, Engel et al. 1997, Sereno et al. 1995), allowing visualization of the polar angle (Fig. 1A, upper panel) and eccentricity (Fig. 1A, lower panel) components of the retinotopic map. The retinotopic map was constructed using a phase-encoding technique where the receptive field centers were temporally coded using polar coordinates (Engel et al. 1994). The polar angle component of the map was measured by performing the fMRI while the subject viewed a wedge-shaped checkered pattern (24° center angle) that rotated counter-clockwise around the fixation point, making one rotation in 60 s. The eccentricity component was measured while the subject viewed a checkered annulus (2° width) that expanded from the fovea to 16° peripherally over 50 s and then disappeared for 10 s. Each stimulus underwent color (black/white, red/green, or blue/yellow) pattern reversal (1 Hz) and was presented in six cycles, evoking a periodic response at a given point on the retinotopy map, where the corresponding position in the visual field was encoded in the phase of the response. The response phase for each of the polar angles or eccentricity components was computed using Fourier analysis and mapped onto the cortical surface (Fig. 1A). More details of the surface reconstruction, the retinotopy mapping, and the parcellation schema have been described elsewhere (H. Yamamoto et al. 2008, Yamamoto et al. 2011).

http://dx.doi.org/10.5772/30760

2.3. Generation of the probability and entropy maps

Quantification of the inconsistency and uncertainty of the locations of the human retinotopic areas in the Talairach space comprised three basic steps: 1) construction of volumetric models of the retinotopic areas, 2) generation of the probability map, and 3) generation of the entropy map, as schematized in Fig. 1. In the first step, volumetric models of the retinotopic areas were constructed for each of the 10 hemispheres by first localizing them on the cortical surface (Fig. 1B) and then converting each area's surface to a volumetric model of 3 mm thickness (Fig. 1C). This conversion began by computing the distance from the surface of each area to the points of an output volume. The distance data was then thresholded at 1.5 mm (half the distance of the assumed thickness) to produce a draft version of the volumetric model for each area. Finally, the draft models of the different areas in one hemisphere were compared to each other to detect where the dilation caused the overlap among them, and the overlapped voxels detected were removed from the models, producing a final volumetric model for each area. The volumetric model is a 3D binary array of voxels, with each voxel having a label indicating the presence or absence of the area. We confirmed that each model did not overlap with the others and had no topological defects, such as discontinuities and holes, by visual inspection of the 3D volume and surface rendered models.

In the second step, the inconsistency associated with each area was assessed as its occurrence probability; that is, in the form of the probability map. For each area, we transformed 10 volumetric models constructed from the 10 hemispheres into Talairach space (Fig. 1D, E) and then counted the number of overlapping models for each anatomic point. We used a single homogeneous transformation (Table 1), which consists of nine parameters, three translations, three rotations, and three scalings with respect to the axes of a Cartesian frame. The homogeneous transformation was determined using a standard method (Desmond & Lim 1997). First, the translation and rotation components of the matrix were computed from the locations of the anatomical landmarks (AC, PC, and mid-sagittal plane) identified by visual inspection of the structural volume. The alignment was checked and corrected by graphically comparing the X-, Y-, and Z-axes with the three orthogonal slices of the standard volume and the reconstructed surface. Next, the scale components were determined by measuring the size of the brain along each of the three axes as the bounding box dimensions of the surface and then computing the scaling factors to match the size to that of the 1988 Talairach atlas brain (X dimension: 136 mm; Y: 172 mm; Z: 118 mm). The scaling factor was determined separately for the left and right hemispheres. Because the Talairach atlas only contains a right hemisphere, the volumetric models for the left hemispheres were mirrored around the Y-axis and treated as though they were in right hemispheres. The occurrence probability of each area of Talairach space was computed by dividing the number of overlaps by the total number of hemispheres ($N = 10$). This computation was repeated every 1 mm in the Talairach space covering the visual cortex, yielding a 3D probability map for each retinotopic area (Fig. 1F). Furthermore, the probability maps for all the retinotopic areas were integrated into a maximum probability map (Fig. 1G) where each voxel was assigned a label indicating which area had the greatest probability of being present there and was given the maximum value.

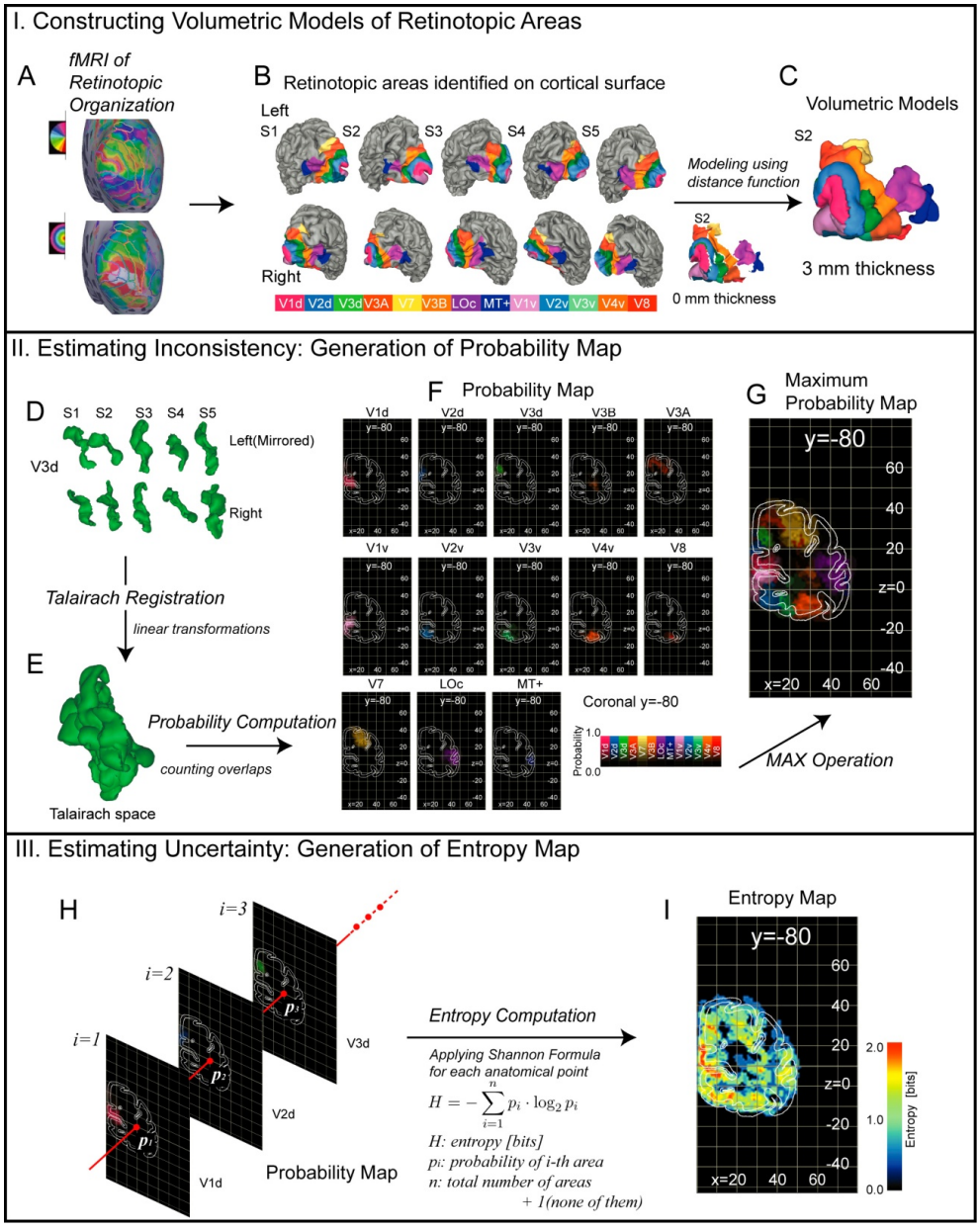

Figure 1. Overview of probabilistic atlas generation. See text for further explanation.

In the final step, the uncertainty associated with the retinotopic areas was assessed in the form of an entropy map (Fig. 1I) by calculating the Shannon entropy (Shannon 1948) from the

occurrence probabilities of the different retinotopic areas (Fig. 1H), where this yields a quantitative measure of the uncertainty represented by a probability distribution. If no uncertainty exists in the distribution, the entropy equals zero, but if the entropy is greater than zero, it is maximal when all events are equally probable. The Shannon entropy (H) of the retinotopic areas can be expressed in terms of the occurrence probabilities (pi) of the different retinotopic areas and is given by

$$H = -\sum_{i=1}^{n} p_i \cdot \log_2 p_i \left[\text{bits}\right], \tag{1}$$

where n is the total number of candidate areas. By applying this equation to the probability maps of the retinotopic areas, we calculated the entropy for each point in the Talairach space covering the visual cortex (Fig. 1H, I). In the present analysis, $n = 14$; each of the 13 retinotopic areas = p_1, p_2,...p_{13} ; plus none of them, p_{14}. Thus, the maximum theoretical value for entropy is

$$-\sum_{i=1}^{14} \frac{1}{14} \log_2 \frac{1}{14} = \log_2 14 \cong 3.8 \left[\text{bits}\right], \tag{2}$$

2.4. Estimating two sources of uncertainty

We estimated two other kinds of entropies underlying the entropy about 14 possible states (retinotopic areas, and non-retinotopic area,) as computed above. The first was the entropy of two possible states, whether a voxel is located anywhere in the retinotopic areas (pr) or located outside of the areas (pnr), which was computed as follows:

$$H_r = -p_r \cdot \log_2 p_r - p_{nr} \cdot \log_2 p_{nr} \left[\text{bits}\right], \tag{3}$$

where

$$p_r = \sum_{i=1}^{13} p_i = 1 - p_{14} \text{ and } p_{nr} = p_{14}. \tag{4}$$

Because H_r is binomial, its maximum theoretical value is 1 bits. This binomial entropy would account for the uncertainty about whether a voxel is located within the visual cortex or is in the white matter, outside the brain or in the non-retinotopic cortex.

The second entropy type was the entropy of retinotopic areas computed on the probability distribution conditioned on a voxel being anywhere in the retinotopic areas, and was computed as follows:

$$H_c = -\sum_{i=1}^{13} p_{i/r} \cdot \log_2 p_{i/r} \left[\text{bits}\right], \tag{5}$$

where the conditional probability $p_{i/r} = p_i\, p_r$ and H_c was computed for voxels with $p_r \geq 0.2$, that is, for voxels that fell within any retinotopic area at least in two of ten hemispheres because it is impossible for areal overlap to occur for a voxel with $p_r = 0.1$. As the conditional entropy H_c has 13 possible states, its maximum theoretical value is

$$-\sum_{i=1}^{13} \frac{1}{13} \log_2 \frac{1}{13} = \log_2 13 \cong 3.7 \left[\text{bits}\right], \tag{6}$$

Please note, unlike the unconditional entropy H, H_c was computed on the probability distribution that did not comprise the event of "a voxel being in non-retinotopic area" and was rather conditional on the event of "a voxel being in retinotopic area". This conditional entropy would thus not be affected by the misalignment of cortical surfaces across hemispheres, and thereby reflect the uncertainty due to variability in the cortical locations of the areas in Talairach space.

2.5. Analysis and visualization software

The analyses were performed and visualized using BrainFactory software (Yamamoto 2011, H. Yamamoto et al. 2008, Yamamoto et al. 2002) written in VTK (Kitware, Clifton Park, NY) and MATLAB (Mathworks, Natick, MA), which has been successfully applied to cortical surface-based analysis of fMRI data (Ban et al. 2006, Ejima et al. 2007, Maeda et al. 2010, Yamamoto et al. 2011, T. Yamamoto et al. 2008) and cortico-cortical evoked potentials (Matsumoto et al. in press).

3. Results

To analyze the interindividual variability in the locations of the visual areas, we created a 3D probability map of the visual areas (e.g., for a coronal slice, see Fig. 1F) where each voxel was associated with the occurrence probabilities (N = 10) for each of the areas. It is difficult to display all such multivariate volume data in only two dimensions, so only the essence of the data is graphically presented in Fig. 2A in the form of a maximum probability map, where each point is color-coded according to the visual area with the greatest frequency (the maximum probability area), and the brightness represents the probability that the area resides at that voxel. The regions of maximal consistency are shown with maximal brightness, and the regions of minimal consistency are shown with minimal brightness. Figure 2A displays this information using the same coronal serial slices as the

http://dx.doi.org/10.5772/30760

1988 atlas of Talairach and Tournoux (1988), overlaid on the Talairach brain, the gray matter of which is outlined using white lines. The probability data in the horizontal and sagittal slices are also shown in Figs. 3A and 4A, respectively.

3.1. Inconsistency in the locations of visual areas: Probability map

The maximum probability area changes within the slices in the same hierarchical order as in the individual hemispheres. This topographic pattern is clearly illustrated in Fig. 5A, which shows the maximum probability map overlaid on the surface representation of the Talairach brain. The topographic preservation can be confirmed, except for the island-like V3 regions within V3B. In contrast to the near complete preservation of the topographic relations of the maximum probability areas, the probability maps of the corresponding areas (e.g., for a coronal slice, see Fig. 1F) revealed substantial inconsistency. As can be partially seen in Figs. 1F, 2A, 3A, and 4A, the probabilistic volume for a corresponding area (voxels having non-zero probabilities) is blurred so strongly that its extent is much wider than the thickness of the cortical gray matter. The strength of this tendency seems to vary among the visual areas, being strongest for area V7/IPS-0, which is located anterior to V3A (Tootell et al. 1998).

Positional inconsistency was quantitatively analyzed, and the results are shown in Fig. 6. Figure 6A illustrates the overall positional inconsistency, showing the distribution of maximum probability values within the voxels containing a non-zero probability. Most of the voxels were associated with small probabilities, with approximately half (47.3%) of them being associated with a value of 0.1 (only a single case representing a visual area) and 96.5% being associated with values less than 0.5 (0.2: 27.0%; 0.3: 15.1%; 0.4: 7.1%). The remaining 3.5% of the voxels were associated with probabilities equal to or larger than 0.5, with the maximum value being not 1.0 but 0.8 (0.5: 2.7%; 0.6: 0.67 %; 0.7: 0.14%; 0.8: 0.007%).

Separate analyses for the individual visual areas were also performed by spatially averaging all of the probability values within each area's probabilistic volume. The average probability is compared among the visual areas in Fig. 6B. The differences were not large, but the average probabilities were slightly lower for the dorsal areas (V3d, V7, and LOc), indicating a higher alignment inconsistency. Area V7 had the lowest values, as expected from the maximum probability map. The overall average of the average probabilities of the areas was 0.166 (SD: 0.013). The coefficient of variance (the SD divided by the mean) was 7.6%.

The analogous alignment inconsistency was evident when using another measure, percent blurring (Fischl et al. 1999b), which is defined as the percentage increase in the probabilistic volume of an area as compared with the mean volume of the individual areas. The percent blurring, which is compared among the visual areas in Fig. 6C, shows a pattern that is nearly reversed compared with the average probability (Fig. 6B), indicating a similar relative inconsistency among the visual areas. The average percent blurring for the group of areas was 460%.

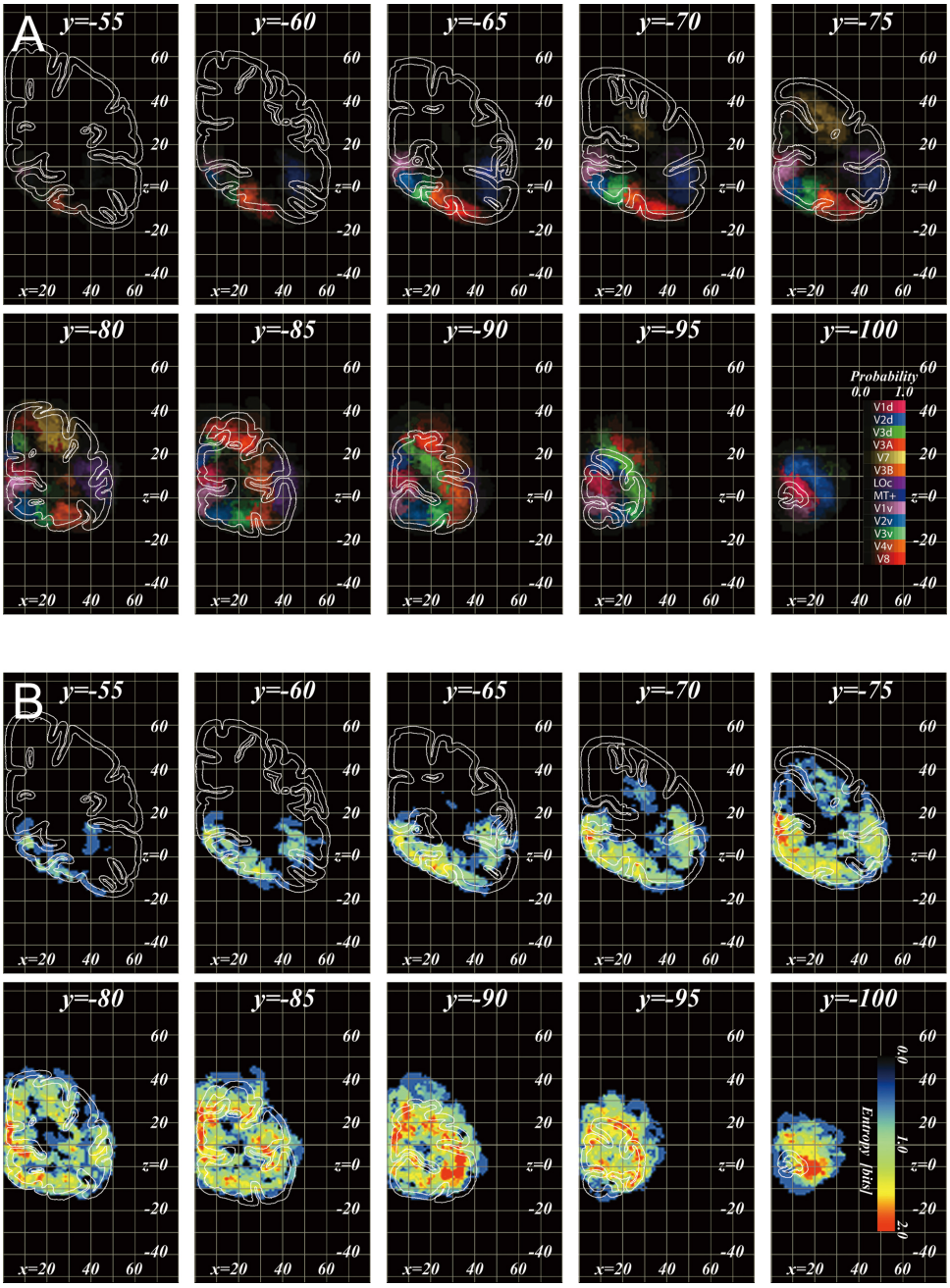

Figure 2. Maximum probability map (A) and entropy map (B) on serial coronal sections.

http://dx.doi.org/10.5772/30760

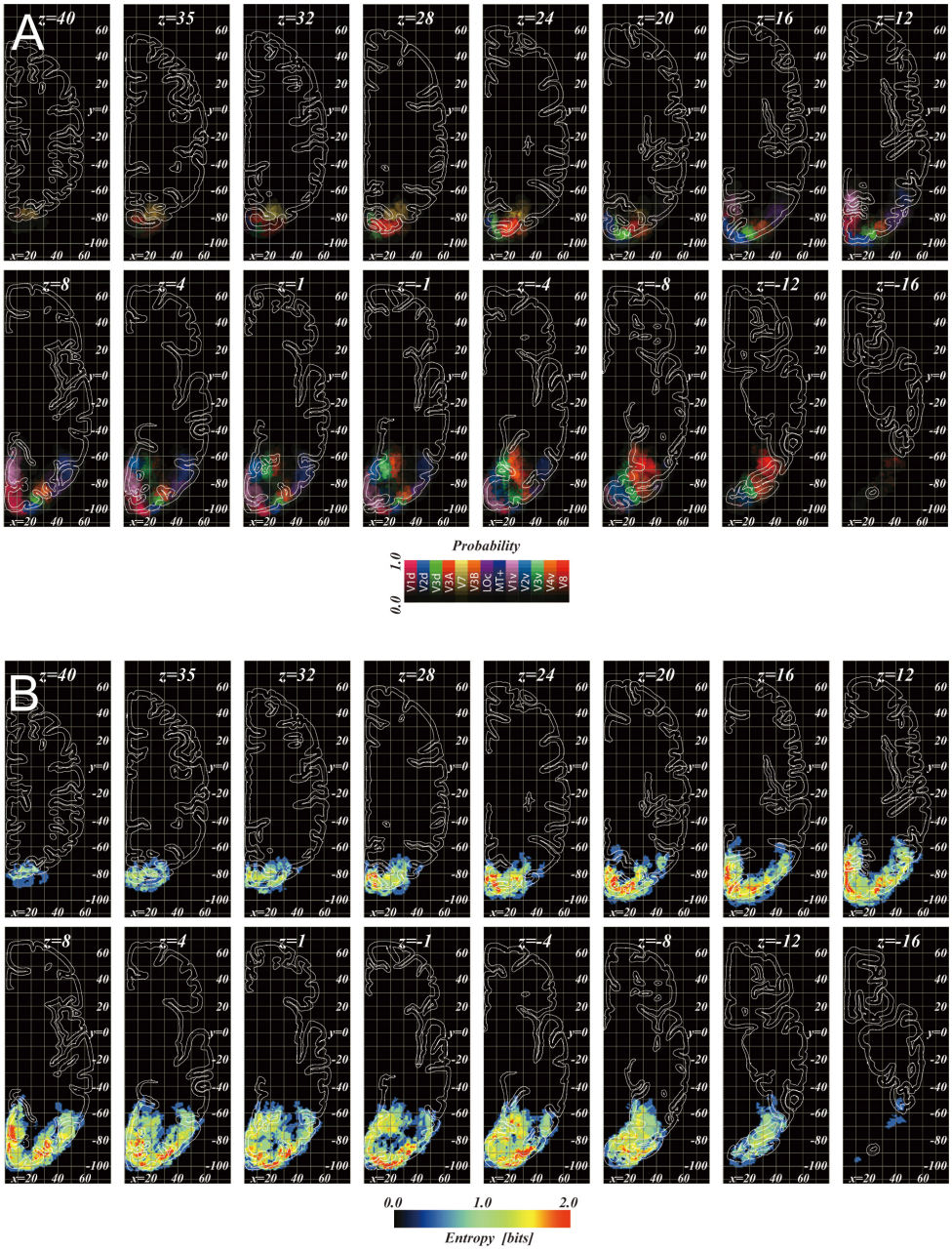

Figure 3. Maximum probability map (A) and entropy map (B) on serial horizontal sections.

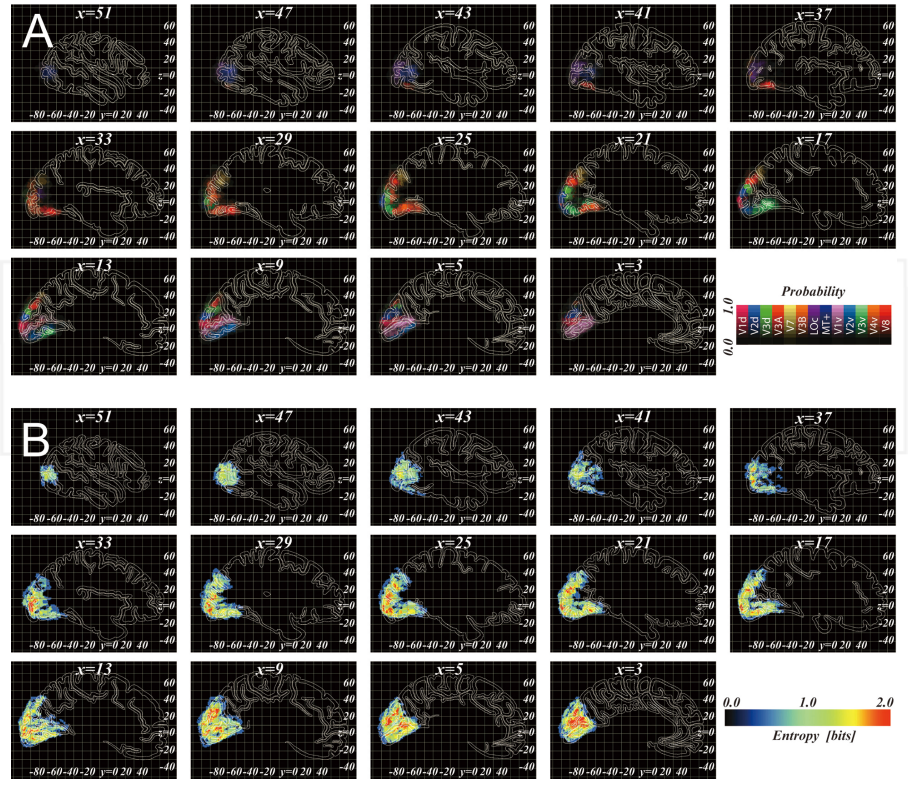

Figure 4. Maximum probability map (A) and entropy map (B) on serial sagittal sections.

3.2. Uncertainty in the locations of visual areas: Entropy map

Next, we performed a series of quantitative analyses regarding the uncertainty about which visual area actually resides at each voxel in Talairach space. As expected, registration of the individual visual areas into the Talairach space led to substantial overlaps among different visual areas. Figure 7A demonstrates this by showing the distribution of the number of overlaps among the areas. When considering the overlaps for all voxels associated with a non-zero probability (71804 voxels), these occurred in nearly half (46.7%) of the voxels and ranged from two to five overlapping areas per voxel (2: 35.4%; 3: 9.8%; 4: 1.5%; 5: 0.04%). Because it is impossible for overlap to occur in a voxel with a 0.1 probability (being in a visual area only for one hemisphere), we also computed the overlaps within the set of voxels with a probability greater than 0.1 (48116 voxels), finding the proportion of overlaps increased to occupy 69.6% of the voxels (2: 52.8%; 3: 14.6%; 4: 2.2%, 5: 0.05%).

To analyze the uncertainty resulting from the overlaps in an information theory framework (Shannon 1948), we introduced the Shannon entropy, a measure of the amount of uncertainty

http://dx.doi.org/10.5772/30760

represented by a probability distribution. In our study, this distribution is the probability of occurrence of the 13 delineated areas plus the probability of occurrence of none of the areas at each voxel in Talairach space. If any of the probabilities is 1.0, such that there is no uncertainty, the Shannon entropy of the visual area is zero, but if not, the entropy is greater than zero. The entropy takes a maximum value of 3.8 bits when the probabilities of all events occurring are the same, such as when we are very uncertain of which of the 14 events has occurred. By applying Shannon's formula to the occurrence probabilities (Fig. 1H, I), we created a 3D map of the entropy of the visual areas within the same occipital region of Talairach space as the probability map.

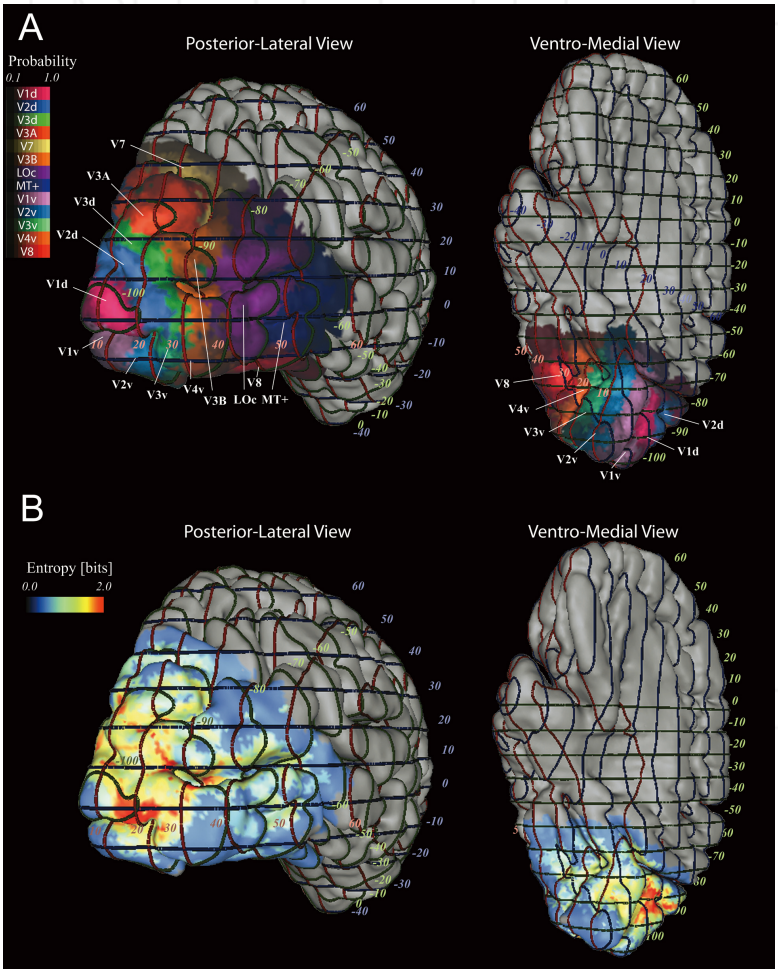

Figure 5. Surface representation of the maximum probability (A) and entropy map (B) of the areas.

Figure 2B/3B/4B shows the entropy map overlaid on the Talairach brain with the same coronal/horizontal/sagittal slice positions as the maximum probability map, where the entropy of the visual area at each voxel is color-coded from blue to red. Figure 5B also shows the entropy map overlaid on the surface representation of the Talairach brain in the same way as the maximum probability map (Fig. 5A). The entropy was less than 2 bits for most voxels, as evidenced by the predominance of blue and yellow regions. As shown in Fig. 7B, the larger the entropy, the smaller the number of voxels. The entropy values ranged from 0.47 to 2.45 bits, with a median value of 0.92 bits.

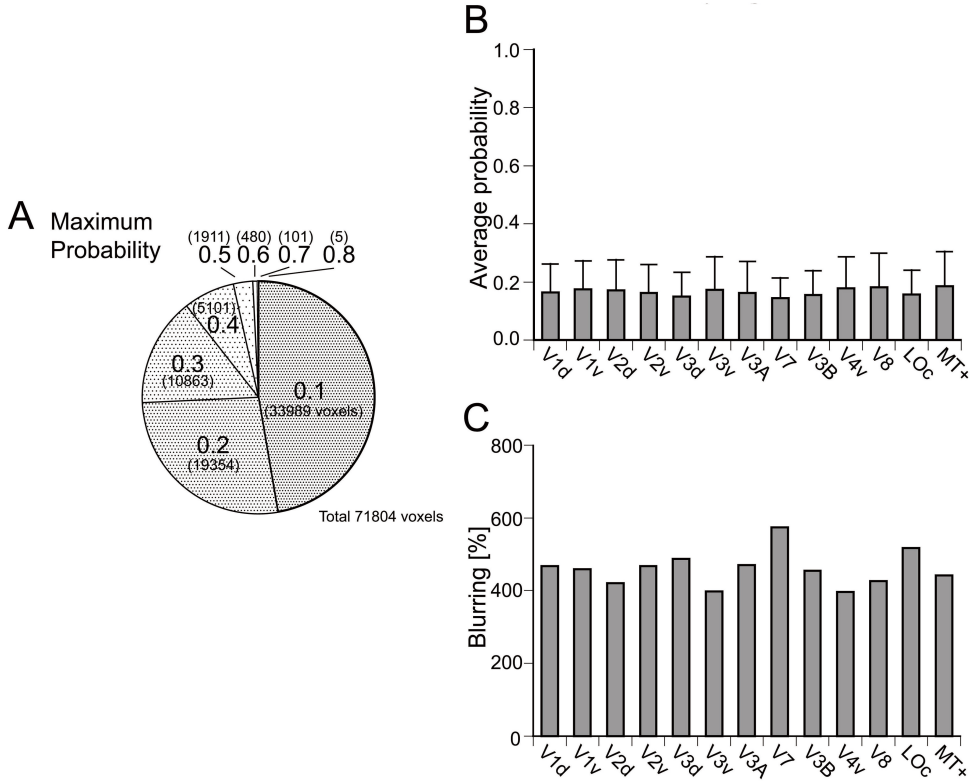

Figure 6. (A) Proportion of the maximum probabilities. The numbers of voxels are indicated in parentheses. (B) Average probability for each visual area across all the area voxels (probabilistic volume) in Talairach space, which is defined as the voxels being classified as an area for at least one hemisphere. Error bars denote SD. (C) Percent blurring of each visual area. This metric measures the amount of increase between the total volume of the area's voxels in its probability map and the mean volume of the area across hemispheres. If registration is perfect, the total volume in Talairach space will be equal to the mean volume, and percent blurring will be zero. For example, a value of 400% means that the total volume of the area's voxels is 5 times as big as the mean volume.

The comparison of the entropy map with the maximum probability map shows a topographical relationship between these. Regions with high entropy values (red) are generally located near

http://dx.doi.org/10.5772/30760

places where multiple visual areas would be located in close proximity, such as the foveal confluence separating the dorsal and ventral region (e.g., [X,Y,Z]=[20,-100,0]) and the borders of areas (e.g., for V3d/V3A/V3B, [20,-90,20]). Conversely, the regions with low entropy values (blue) tend to lie outside of the crowded fields.

Entropy is conceptually and computationally distinct from maximum probability, such that its map has a unique importance. However, if these measures were empirically related to each other, the entropy map would become less important. For a potential relationship, one would expect that high entropy would generally be associated with a low probability of belonging to one area. Therefore, we examined the relationship between entropy and maximum probability on a voxel-by-voxel basis, but found no correlation consistent throughout their range (Fig. 8). Although the expected negative correlation was observed for the higher maximum probability levels (0.4—0.8), the number of voxels in the range occupied only 11% of all the area's voxels. The entropies of the voxels with lower probability levels, which occupied the remaining 89% of the voxels, dispersed widely and showed rather positive correlations with maximum probabilities. Consequently, the entropy provides information distinct from that conveyed by the maximum probability, which emphasizes the importance of the entropy map.

We also quantified the uncertainty at the level of the visual areas by averaging all of the entropy values within the probabilistic volume of each area. The average entropy is compared among the areas in Fig. 7C. The average entropy was smaller, less than 1 bit, for areas V7, V8, LOc and MT+, and was at a minimum for MT+. For other areas, the average entropy was greater than 1 bit and was at a maximum for V2d. The difference between the maximum and minimum was 0.47 bits. The average entropy for the group of areas was 1.07 bits (SD: 0.175). The coefficient of variance was 16.4%, which is about two-fold larger than the probability.

Comparison of the average entropy (Fig. 7C) with the average occurrence probability (Fig. 6B) and blurring (Fig. 6C) shows the dissociation between uncertainty and inconsistency at the cortical area level. For example, areas V7 and V8 display opposite patterns: V7 has the smallest average probability, the largest blurring, and the second smallest entropy value, whereas V8 has a relatively large average probability, small blurring, and comparable entropy with V7; thus, V7 exhibits relatively strong inconsistency with relatively small uncertainty, whereas V8 exhibits relatively weak inconsistency with relatively small uncertainty. As complementary examples, V3d exhibits relatively strong inconsistency with relatively large uncertainty, whereas V2d exhibits relatively small inconsistency with relatively large uncertainty.

3.3. Two sources of uncertainty in the locations of visual areas

Finally, we analyzed the potential sources of the areal uncertainty. There are at least two sources of entropy when computed over the probability distribution of 14 possible states (13 areas plus none of them), as stated above. The first is the uncertainty as to whether a voxel is located within the visual cortex or lies within the white matter, outside the brain, or in non-retinotopic areas. We estimated this cortical registration factor by computing the entropy over the probability distribution of two events of the "voxel being in any of retinotopic areas" or not. Figure 9A compares the estimated entropy (theoretical maximum, 1 bit) among the retinotopic areas. Although the binomial entropy was a little smaller for area V7, it was nearly

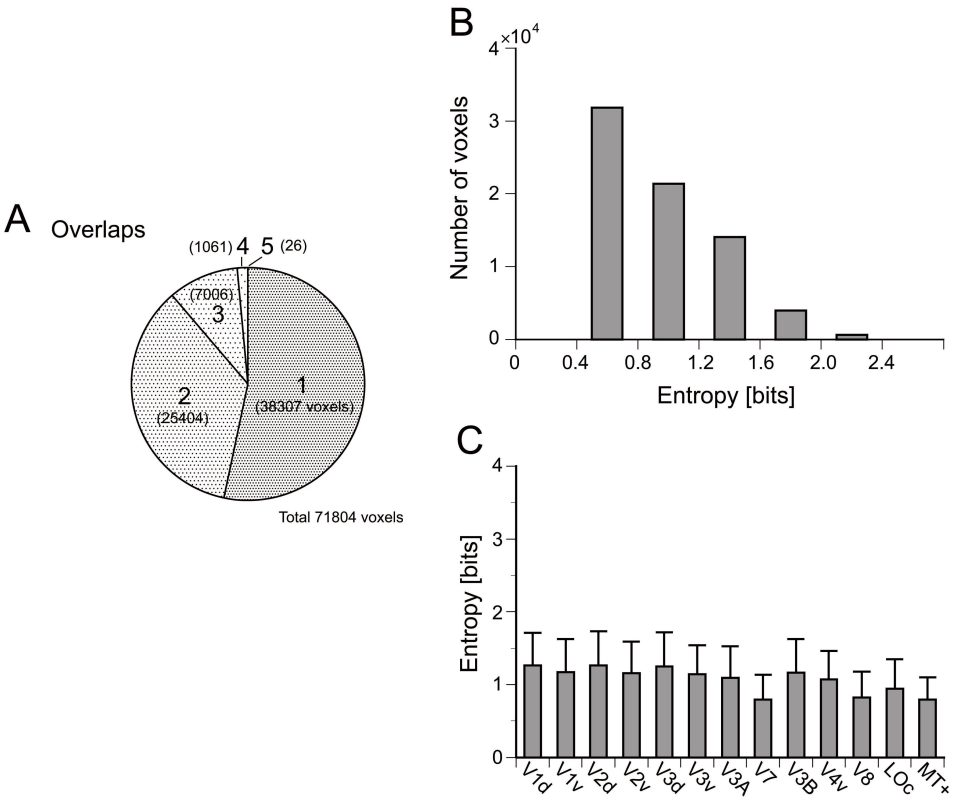

Figure 7. (A) Proportion of the number of overlaps among different visual areas in Talairach space. For example, an "overlap" of 1 means that these voxel correspond uniquely to a single area, whereas overlaps of 2 means that these voxel correspond two areas (one area for some hemispheres but another area for the other hemispheres). (B) Histogram of the entropy values. (C) Average entropy of each visual area across all the area's voxels (probabilistic volume). Error bars denote SD.

constant across the areas, as indicated by the fact that the standard deviation (0.022) was only 2.5% of the mean (0.87). The coefficient of variance was much smaller, by a factor of 6.4, compared with the result of the entropy over the full distribution of the 14 possible states (Fig. 5C). Therefore, this factor of uncertainty alone cannot explain the entropy difference among retinotopic areas.

The second factor was the uncertainty that remains even after the removal of the first uncertainty due to the registration, such as after knowing a voxel was being registered to some part of the retinotopic visual cortex. We estimated this by computing the entropy over the probability distribution of the retinotopic areas conditioned on a voxel belonging to any of the areas. This conditional entropy would reflect the underlying intersubject variability in the location on the cortical surface. Figure 9B compares the estimated conditional entropy (theoretical

http://dx.doi.org/10.5772/30760

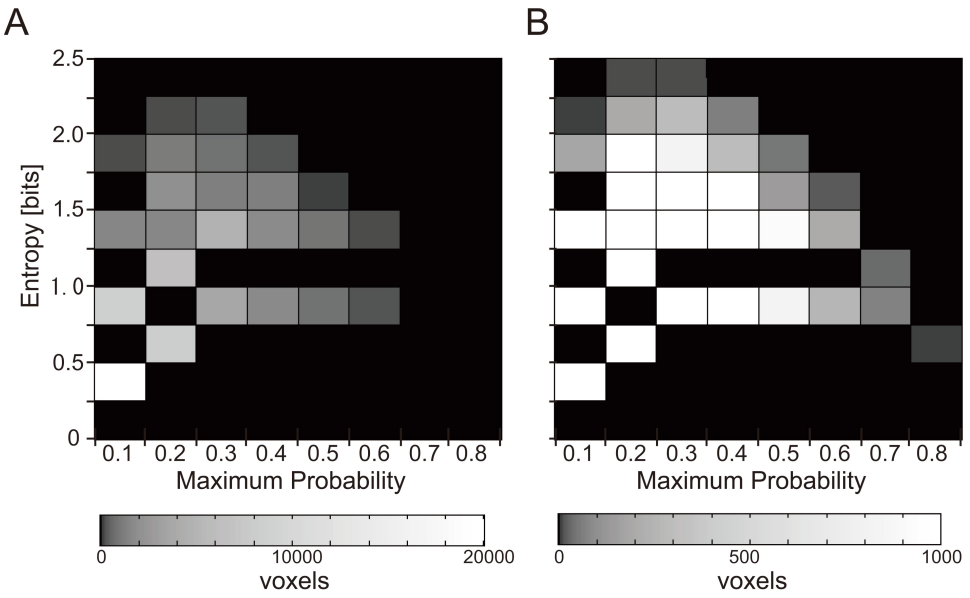

Figure 8. Two-dimensional histogram of entropy vs. maximum probability for all the area voxels. The histogram assigns a brightness value to each bin based on the number of voxels. The brighter the bin, the greater the number of voxels in that range. The brightness scale ranges from 0 to 20000 voxels. (B) Same histogram image as in A with a different, narrower scale to emphasize small differences in the number of voxels. The scale ranges from 0 to 1000 voxels.

maximum, 3.7 bits) among the retinotopic areas. Unlike the first binomial entropy due to cortical registration (Fig. 9A), the conditional entropy showed a substantial difference among the retinotopic areas, as indicated by a coefficient of variance of 27.6% (mean, 0.89; SD, 0.246), which was much larger, by a factor of 10.9, than the first entropy. The approximate ten-fold difference in the two entropy measures remained even when the comparison was limited to lower retinotopic areas, excluding the higher areas, V7, V8, LOc, and MT+, which are enclosed by more non-adjacent borders (coefficient of variance, 10.9% vs. 1.1%). Notably, the pattern of the difference among the areas (Fig. 9B) was similar to that found for the non-conditional entropy (Fig. 7C) but with more pronounced variability. The coefficient of variance and the difference between the maximum and minimum were larger, by factors of 1.7 and 1.6, respectively, than those obtained for the non-conditional entropy.

4. Discussion

The Talairach coordinate system has inherent limits in reducing the interindividual variability in the complex topography of the brain structure. The purpose of the present study was to apply a probabilistic and information theoretical framework for analyzing the residual interindividual variability of human visual area loci in Talairach space. The key feature of the

framework is its ability to quantify the complementary aspects of the interindividual variability, inconsistency and uncertainty by constructing probability and entropy maps. The inconsistency and uncertainty of the locations of retinotopic areas found by analysis using this framework will be discussed below. In addition, we will discuss the applications of the maps and the framework.

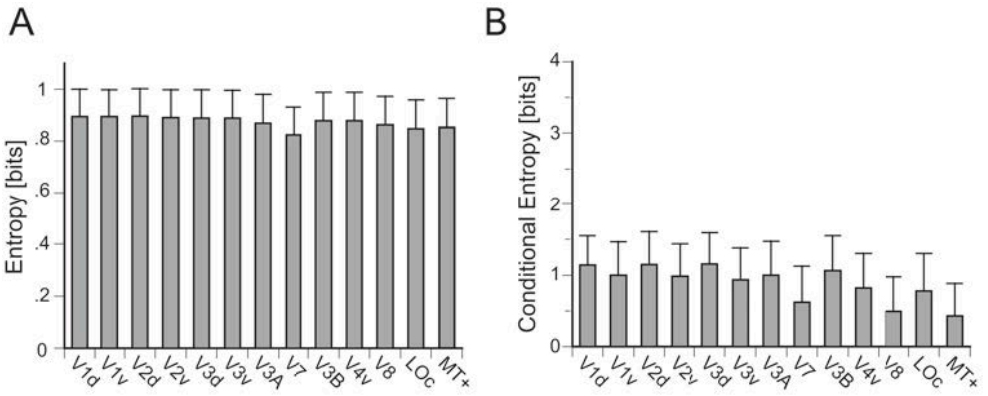

Figure 9. (A) Entropy computed on probability distribution whether a voxel is located in any retinotopic area or not. (B) Entropy computed on areal probability distribution *conditioned* on a voxel being in the visual cortex (retinotopic area). Error bars denote SD.

4.1. Inconsistency in the locations of visual areas: Probability map

In the present study, the alignment inconsistency of retinotopic areas (V1d/v, V2d/v, V3d/v, V4v, V8, V3A, V3B, V7, LOc, and MT+) was analyzed using a probabilistic approach (Mazziotta et al. 1995, Roland & Zilles 1994). The comprehensive application of this approach to visual areas was pioneered by Van Essen et al. (2001), who constructed probability maps of multiple areas (V1d/v, V2d/v, V3d/v, V3A, V4v, V8, MT+) identified using fMRI data from four hemispheres, using nonlinear surface warping in terms of the landmark coregistration rather than the standard linear Talairach transformation. Recently, we have also created probability maps using a similar surface based-method (Yamamoto et al. 2011). In this study, we generated probability maps of multiple retinotopic areas using standard linear Talairach transformation. Such maps have been made for the cytoarchitectonic definitions of areas V1 and V2 in five (Roland et al. 1997) and 10 brains (Amunts et al. 2000) and areas V3v and V4v in ten brains (Rottschy et al. 2007). Cytoarchitectonic studies of V1 and V2 have demonstrated that the probability volume of V2 surrounds that of V1 with substantial overlap, implying that the inconsistency was large, but not so large as to grossly violate the positional relationship. Our probability maps extend the observation to multiple functionally-defined visual areas.

Regarding the comparison across areas, it has been noted in cytoarchitectonic studies (Amunts et al. 2000) that the degree of inconsistency is smaller for V1 than for V2. However, such a pattern was not detected using the percent blurring measure in another study using fMRI

http://dx.doi.org/10.5772/30760

(Fischl et al. 1999b), where the comparison was made among V1d/v, V2d/v, and MT+. Consistent with this, the percent blurring measured in this study did not differ greatly among these areas. The discrepancy between anatomical and functional results may be resolved by examining them together using a common measure. One such integrated approach has been recently applied to areas V1 and V2 using probability maps, showing consistent results between the anatomical and functional probability maps (Wohlschlager et al. 2005). However, there appears to be a tendency for interindividual variability of the areas to increase in the anatomical map (see Fig. 5 in the study). Further studies are needed to elucidate the reason for this small discrepancy.

We also made a comparison across areas, introducing an intuitive measure of the average probability. Although the difference was not marked, we found slightly smaller average probabilities for areas V3d, V7, and LOc than for the other areas. A possible explanation is that as these areas are often buried in deep sulci, namely the intraparietal sulcus and lateral occipital sulcus, and that small differences in the courses of the sulci may prevent these areas from overlapping between the different subjects. The grand average across all areas was found to be only a little under 0.2, indicating substantial inconsistency.

4.2. Uncertainty in the locations of visual areas: Entropy map

Whereas the probability map allowed us to determine how probable it is that a particular visual area resides at a set of Talairach coordinates, the entropy map allowed us to quantify the uncertainty about the set of probability events. It should be stressed that even if events are highly probable, the entropy is large when the different events occur simultaneously, such as when the different areas overlap. The significance of the entropy map is in this dissociation. Indeed, our voxel-wise analysis of the relationship between the entropy and the maximum probability maps (Fig. 8) revealed that these statistics are largely unrelated, empirically supporting the dissociation of human visual areas in Talairach space. Although this dissociation has not been explicitly examined, the overlap between different structures has been noted previously in the context of the brain registration. Roland et al. (1997) identified areas V1 and V2 cytoarchitectonically and reported that the overlap between V1 and V2 is as large as the overlap between the different V1 areas. Van Essen (2005) analyzed the degree of overlap between the neighboring brain sulci using a probability map. Importantly, these studies all disregarded the occurrence probabilities of the overlapping structures, despite the uncertainty being maximal when each event is equiprobable. The present study extends these earlier analyses by relating the probabilities to the concept of uncertainty using entropy.

We found that the overall average of the entropy of retinotopic areas is approximately 1 bit in Talairach space, indicating that there are, on average, 1 bits of uncertainty about which retinotopic area is present at a point when its Talairach coordinates are specified. This means that there is an equal chance of each area being present for a point where two areas overlap. As for the spatial pattern of entropy distribution, the entropy map is not isotropic; it contains larger values around the borders of retinotopic areas and smaller values around their non-adjacent borders, which is expected given the possibility of overlaps between the different areas. In addition, we found that there is also a variation in entropy among retinotopic areas.

4.3. Two sources of uncertainty in the locations of visual areas

What causes the areal entropy and its variation in Talairach space? One possibility might be the poor alignment of the cortex under the simple Talairach volumetric registration because the probability distribution on which the entropy is computed contains information about whether a voxel belongs to the cortex. Indeed, the weakness of Talairach normalization is commonly agreed upon, and a prior probabilistic atlas of the human visual areas has been created using surface-based registration to partly overcome this problem (Van Essen et al. 2001, Yamamoto et al. 2011). The present study estimated the uncertainty caused by the inadequacy of Talairach registration by using the binomial entropy as either 'a voxel being in retinotopic area' or not and found that the measure is nearly constant among retinotopic areas. This suggests that the uncertainty due to registration is not a major factor underlying the uncertainty about retinotopic areas in Talairach space, thereby suggesting that the uncertainty due to intersubject variability in the relative size or cortical location of distinct areas (Dougherty et al. 2003, Ejima et al. 2003, Van Essen et al. 2001, Yamamoto et al. 2011) would be a significant factor.

This source of variability is, however, is not well understood. Therefore, we estimated this by computing the entropy for the probability distribution conditioned on a voxel in the cortex. Another approach could apply our non-conditional entropy measure to a surface-based group averaged brain, but this is beyond the scope of the present work. In addition, this method would lose some generality because the surface registration generally requires a set of anatomical or functional landmarks, and their selection would affect entropy. In contrast, our conditional entropy only assumes the association of a voxel to the cortex, such that it would constitute a baseline measure of the uncertainty remaining after surface-based normalization. The conditional entropy averaged across retinotopic areas was found to decrease by approximately 10%, supporting the general advantage of the surface-based normalization over Talairach normalization. This improvement would increase for the existing surface-based methods (Drury et al. 1996, Fischl et al. 1999b, Thompson et al. 1997) because they apply to the individual variability of gyral patterning. We also found that the difference in entropy across areas was amplified upon conditioning. This amplification underlines the fact that entropy provides information distinct from probability and confirms that the uncertainty due to intersubject variability in the layout of the cortical areas is a primary cause of the areal uncertainty in Talairach space. The much smaller observed conditional entropy of several higher areas confirms this idea because they are enclosed by many non-adjacent borders. However, with the exception of the apparent adjacency, we cannot specify the exact reason for the modest variations observed in lower retinotopic areas.

4.4. Preliminary comparison among registration methods

Three types of registration methods are commonly used, namely the linear volume-based, nonlinear volume-based, and surface-based methods. Among these, we evaluated a linear volume-based method for 5 subjects in the present study and a surface-based method for 16 subjects in a recent study (Yamamoto et al. 2011). Extending these studies, we initiated a comparison study among the three types of methods. Table 2 shows a preliminary summary

of the results obtained for 16 subjects. As used in the present study, the linear volume-method is a single linear transformation; the nonlinear volume-based method used is an automated image registration (AIR) method (Woods et al. 1998) where a 12 parameter affine linear transformation was followed by a second-order 30 parameter, nonlinear polynomial model; the surface-based method used is an Automated Spherical Warping (Fischl et al. 1999b) of the FreeSurfer software package (Dale et al. 1999, Fischl et al. 1999a), which displaced the vertices of each labeled surface to match its folding pattern with that of the FreeSurfer average template surface. As expected, the surface-based method gave the best results for probability. However, surprisingly, the surface-based method lost its advantage for entropy (average entropy: ~ 1 bits). This suggests that the current technology is not perfect and should therefore be used with caution regarding the limits.

	Linear volume-based method	Nonlinear volume-based method	Surface-based method
Average probability	0.089 (0.016)	0.10 (0.013)	0.27 (0.074)
Average entropy [bits]	1.01 (0.18)	1.07 (0.20)	1.15 (0.23)

The average probability(entropy) over 12 areas (V1, V2d, V2v, V3d, V3v, V3A, V7, V3B, V4v, V8, LOc, MT+) was listed. Parenthesis indicates SD across the areas. 16 subjects' brain were coregistered with the three method (see text for description of the methods).

Table 2. Preliminary comparison among registration methods

4.5. Applications

The present probabilistic and information theoretical framework has a variety of applications related to interindividual variability in the human brain. Probability and entropy maps of retinotopic areas can readily benefit any application where it is necessary to predict which areas are present at an anatomical point with a high probability and to establish the uncertainty associated with the prediction given its Talairach coordinates. Using these maps, the researchers and clinicians can infer, with a known degree of uncertainty, the visual area that is most likely present at an activation site or a lesion site within a target brain for which any form of the direct identification is impossible. The non-conditional entropy is a useful measure of the uncertainty observed in a practical situation, such as to average functional activations for different subjects or regimens for stereotaxic surgical treatment, whereas the conditional entropy allows a more fundamental appreciation of uncertainty regarding the cortical location of visual areas when analyzing the layout and network of cortical areas. The other main application is in the field of brain registration and brain warping (Toga 1999). As demonstrated in this study, Talairach registration reduced the entropy of visual areas from approximately 4 bits to 1 bit. In this way, the performance of various registration methods can be compared quantitatively using the degree of reduction in the entropy of the structures to be coregistered. Finally, the present work on visual areas can be generalized to not only other functional structures, but also other anatomical structures. Thus, an important direction for future

research is to extend the present framework to address brain structure-function relationships, which are the focus of an ongoing large-scale international project that aims to develop a probabilistic brain atlas representing many types of information on brain function and structure (Mazziotta et al. 2001). One such approach is quantifying relationships using the Shannon mutual information based on simultaneous probability maps of structural and functional areas (Yamamoto et al. 2003).

5. Conclusion

We made two kinds of multisubject maps (10 hemispheres from five subjects) to characterize interindividual variability in the positions of human visual areas (V1/2/3, V3A, V3B, V7, V4v, V8, LOc, and MT+), which were localized using fMRI and coregistered into standard Talairach space by a single linear transformation. The first is a probability map representing the amount of alignment inconsistency for each area, where each voxel in space is associated with a probability affiliated with a given area. The second, a novel map termed an entropy map where each voxel is associated with a Shannon entropy computed from the probabilities, represents the amount of uncertainty that exists regarding which area resides there and is maximal when all areas are equally probable. We demonstrate that the entropy map provides distinctly different information from the probability map, highlighting the significance of the entropy map. The overall average probability and entropy values were ~0.2 and ~1.0 bits, respectively, with some area differences. The difference increased when computing the entropy for the probability distribution conditioned on a voxel located anywhere in the visual cortex, suggesting that a major source of the observed uncertainty is not due to the poor alignment of the cortex, but to individual variability in the cortical locations of the visual areas. The probability and entropy maps generated in this study will readily benefit any application where it is necessary to predict the areas that are most likely present at an anatomical voxel and to establish the uncertainty associated with this prediction.

Acknowledgements

This work was supported by Grant-in-Aids for Global COE (Centers of Excellence) Program (D07), Scientific Research on Innovative Areas (No. 22135007), and Scientific Research (C) (No. 22530793) of Japan's Ministry of Education, Culture, Sports, Science and Technology.

Author details

Hiroki Yamamoto*

Graduate School of Human and Environmental Studies, Kyoto University, Japan

http://dx.doi.org/10.5772/30760

References

[1] Amunts K, Malikovic A, Mohlberg H, Schormann T & Zilles K. (2000). Brodmann's areas 17 and 18 brought into stereotaxic space-where and how variable? *NeuroImage,* Vol.11, No.1, pp. 66-84, ISSN 1053-8119

[2] Ashburner J. (2007). A fast diffeomorphic image registration algorithm. *NeuroImage,* Vol.38, No.1, pp. 95-113, ISSN 1053-8119

[3] Ban H, Yamamoto H, Fukunaga M, Nakagoshi A, Umeda M, Tanaka C & Ejima Y. (2006). Toward a common circle: interhemispheric contextual modulation in human early visual areas. *The Journal of neuroscience,* Vol.26, No.34, pp. 8804-9, ISSN 0270-6474

[4] Cencov NN. (1982). *Statistical decision rules and optimal inference*, American Mathematical Society, ISBN 0821845020, Providence, R.I.

[5] Dale AM, Fischl B & Sereno MI. (1999). Cortical surface-based analysis. I. Segmentation and surface reconstruction. *NeuroImage,* Vol.9, No.2, pp. 179, ISSN 1053-8119

[6] Dale AM & Sereno MI. (1993). Improved localization of cortical activity by combining EEG and MEG with MRI cortical surface reconstruction: A linear approach. *J Cogn Neurosci,* Vol.5, No.2, pp. 162-76, ISSN 1530-8898

[7] Desmond JE & Lim KO. (1997). On- and offline Talairach registration for structural and functional MRI studies. *Human Brain Mapp,* Vol.5, No.1, pp. 58-73, ISSN 1097-0193

[8] DeYoe EA, Bandettini P, Neitz J, Miller D & Winans P. (1994). Functional magnetic resonance imaging (FMRI) of the human brain. *J Neurosci Methods,* Vol.54, No.2, pp. 171-87, ISSN 0165-0270

[9] Dougherty RF, Koch VM, Brewer AA, Fischer B, Modersitzki J & Wandell BA. (2003). Visual field representations and locations of visual areas V1/2/3 in human visual cortex. *J Vis,* Vol.3, No.10, pp. 586-98, ISSN 1534-7362

[10] Drury HA, Van Essen DC, Anderson CH, Lee CW, Coogan TA & Lewis JW. (1996). Computerized mappings of the cerebral cortex: a multiresolution flattening method and a surface-based coordinate system. *Journal of Cognitive Neuroscience,* Vol.8, No.1, pp. 1-28, ISSN 1530-8898

[11] Drury HA, Van Essen DC, Corbetta M & Snyder AZ. (1999). Surface-based analyses of the human cerebral cortex., In: *Brain Warping* AW Toga, pp. 337-63, Academic Press, ISBN 0126925356, San Diego

[12] Ejima Y, Takahashi S, Yamamoto H, Fukunaga M, Tanaka C, Ebisu T & Umeda M. (2003). Interindividual and interspecies variations of the extrastriate visual cortex. *Neuroreport,* Vol.14, No.12, pp. 1579-83, ISSN 0959-4965

[13] Ejima Y, Takahashi S, Yamamoto H & Goda N. (2007). Visual Perception of Contextual Effect and Its Neural Correlates In: *Representation and Brain*, S Funahashi, pp. 3-20, Springer Verlag, ISBN 978-4-431-73020-0, Tokyo

[14] Engel SA, Glover GH & Wandell BA. (1997). Retinotopic organization in human visual cortex and the spatial precision of functional MRI. *Cereb Cortex,* Vol.7, No.2, pp. 181-92, ISSN 1047-3211

[15] Engel SA, Rumelhart DE, Wandell BA, Lee AT, Glover GH, Chichilnisky EJ & Shadlen MN. (1994). fMRI of human visual cortex. *Nature,* Vol.369, No.6481, pp. 525, ISSN 0028-0836

[16] Fischl B, Sereno MI & Dale AM. (1999a). Cortical surface-based analysis. II: Inflation, flattening, and a surface-based coordinate system. *NeuroImage,* Vol.9, No.2, pp. 195-207, ISSN 1053-8119

[17] Fischl B, Sereno MI, Tootell RB & Dale AM. (1999b). High-resolution intersubject averaging and a coordinate system for the cortical surface. *Hum Brain Mapp,* Vol.8, No.4, pp. 272-84, ISSN 1097-0193

[18] Gholipour A, Kehtarnavaz N, Briggs R, Devous M & Gopinath K. (2007). Brain Functional Localization: A Survey of Image Registration Techniques. *Medical Imaging, IEEE Transactions on,* Vol.26, No.4, pp. 427-51, ISSN 0278-0062

[19] Hasnain MK, Fox PT & Woldorff MG. (1998). Intersubject variability of functional areas in the human visual cortex. *Hum Brain Mapp,* Vol.6, No.4, pp. 301-15, ISSN 1097-0193

[20] Lorensen W, E. & Cline H, E. . (1987). *Marching cubes: A high resolution 3D surface construction algorithm.* Proceedings of the 14th annual conference on Computer graphics and interactive techniques, ISBN 0897912276, Anaheim, California, July 27-31, 1987

[21] Maeda K, Yamamoto H, Fukunaga M, Umeda M, Tanaka C & Ejima Y. (2010). Neural correlates of color-selective metacontrast in human early retinotopic areas. *Journal of Neurophysiology,* Vol.104, No.4, pp. 2291-301, ISSN 0022-3077

[22] Matsumoto R, Ikeda A, Fumuro T, Mikuni N, Miyamoto S, Fukuyama H, Takahashi R, Najm I, Shibasaki H & Luders H. (in press). Parieto-frontal network in humans studied by cortico-cortical evoked potential. *Human Brain Mapping*, ISSN 1097-0193

[23] Mazziotta J, Toga A, Evans A, Fox P, Lancaster J, Zilles K, Woods R, Paus T, Simpson G, Pike B, Holmes C, Collins L, Thompson P, MacDonald D, Iacoboni M, Schormann T, Amunts K, Palomero-Gallagher N, Geyer S, Parsons L, Narr K, Kabani N, Le Goualher G, Boomsma D, Cannon T, Kawashima R & Mazoyer B. (2001). A probabilistic atlas and reference system for the human brain: International Consortium for Brain Mapping (ICBM). *Philos Trans R Soc Lond B Biol Sci,* Vol.356, No.1412, pp. 1293-322, ISSN 0962-8436

http://dx.doi.org/10.5772/30760

[24] Mazziotta JC, Toga AW, Evans A, Fox P & Lancaster J. (1995). A probabilistic atlas of the human brain: theory and rationale for its development. The International Consortium for Brain Mapping (ICBM). *NeuroImage,* Vol.2, No.2, pp. 89-101, ISSN 1053-8119

[25] Ono M, Kubik S & Abernathey C. (1990). *Atlas of the Cerebral Sulci*, Thieme, ISBN 0865773629, Stuttgart, Germany

[26] Roland PE, Geyer S, Amunts K, Schormann T, Schleicher A, Malikovic A & Zilles K. (1997). Cytoarchitectural maps of the human brain in standard anatomical space. *Human Brain Mapping,* Vol.5, No.4, pp. 222-27, ISSN 1097-0193

[27] Roland PE & Zilles K. (1994). Brain atlases--a new research tool. *Trends Neurosci,* Vol. 17, No.11, pp. 458-67, ISSN 0166-2236

[28] Rottschy C, Eickhoff SB, Schleicher A, Mohlberg H, Kujovic M, Zilles K & Amunts K. (2007). Ventral visual cortex in humans: Cytoarchitectonic mapping of two extrastriate areas. *Hum Brain Mapp*, Vol.28, No.10, pp. 1045-1059, ISSN 1065-9471

[29] Sereno MI, Dale AM, Reppas JB, Kwong KK, Belliveau JW, Brady TJ, Rosen BR & Tootell RB. (1995). Borders of multiple visual areas in humans revealed by functional magnetic resonance imaging. *Science,* Vol.268, No.5212, pp. 889-93, ISSN 0036-8075

[30] Shannon CE. (1948). The mathematical theory of communication, I and II. *Bell System technical journal,* Vol.27, pp. 379-443

[31] Talairach J, Szikla G, Tournoux P, Prosalentis A, Bordas-Ferrier M, Covello L, Iacob M & Mempel E. (1967). *Atlas d'anatomie stereotaxique du telencephale.*, Masson, Paris

[32] Talairach J & Tournoux P. (1988). *Co-Planar Stereotactic Atlas of the Human Brain*, Thieme, ISBN 978-0865772939, Stuttgart/New York

[33] Teo PC, Sapiro G & Wandell BA. (1997). Creating connected representations of cortical gray matter for functional MRI visualization. *IEEE Transactions on Medical Imaging,* Vol.16, No.6, pp. 852-63, ISSN 0278-0062

[34] Thompson PM, MacDonald D, Mega MS, Holmes CJ, Evans AC & Toga AW. (1997). Detection and mapping of abnormal brain structure with a probabilistic atlas of cortical surfaces. *J Comput Assist Tomogr,* Vol.21, No.4, pp. 567-81, ISSN 0363-8715

[35] Toga AW. (1999). *Brain warping*, Academic Press, ISBN 0126925356, San Diego

[36] Tootell RB, Hadjikhani N, Hall EK, Marrett S, Vanduffel W, Vaughan JT & Dale AM. (1998). The retinotopy of visual spatial attention. *Neuron,* Vol.21, No.6, pp. 1409-22, ISSN 0896-6273

[37] Van Essen DC. (2005). A Population-Average, Landmark- and Surface-based (PALS) atlas of human cerebral cortex. *NeuroImage,* Vol.28, No.3, pp. 635-62, ISSN 1053-8119

[38] Van Essen DC, Lewis JW, Drury HA, Hadjikhani N, Tootell RB, Bakircioglu M & Miller MI. (2001). Mapping visual cortex in monkeys and humans using surface-based atlases. *Vision Res,* Vol.41, No.10-11, pp. 1359-78, ISSN 0042-6989

[39] Wohlschlager AM, Specht K, Lie C, Mohlberg H, Wohlschlager A, Bente K, Pietrzyk U, Stocker T, Zilles K, Amunts K & Fink GR. (2005). Linking retinotopic fMRI mapping and anatomical probability maps of human occipital areas V1 and V2. *NeuroImage,* Vol.26, No.1, pp. 73-82, ISSN 1053-8119

[40] Woods RP, Grafton ST, Watson JD, Sicotte NL & Mazziotta JC. (1998). Automated image registration: II. Intersubject validation of linear and nonlinear models. *J Comput Assist Tomogr,* Vol.22, No.1, pp. 153-165, ISSN 0363-8715

[41] Yamamoto H. (2011) BAVIEW: software for visualization and analysis of probabilistic atlases of human visual areas. *ESMRMB 2011,* Leipzig, DE, Oct. 6-8, 2011

[42] Yamamoto H, Ban H, Fukunaga M, Umeda M, Tanaka C & Ejima Y. (2008). Large- and Small-Scale Functional Organization of Visual Field Representation in the Human Visual Cortex., In: *Visual Cortex: New Research.*, TA Portocello, RB Velloti, pp. 195-226, Nova Science Publisher, ISBN 1604565306, New York

[43] Yamamoto H, Fukunaga M, Takahashi S, Mano H, Tanaka C, Umeda M & Ejima Y. (in press). Inconsistency and uncertainty of the human visual area loci following surface-based registration: Probability and Entropy Maps. *Human Brain Mapping*, doi: 10.1002/hbm.21200, ISSN 1065-9471

[44] Yamamoto H, Fukunaga M, Takahashi S, Tanaka C, Ebisu T, Umeda M & Ejima Y. (2002) BrainFactory: an integrated software system for surface-based analysis of fMRI data. *Human Brain Mapping 2002,* Sendai, Japan, June 2-6, 2002

[45] Yamamoto H, Fukunaga M, Tanaka C, Ebisu T, Umeda M & Ejima Y. (2003) A New Method for Quantifying Brain Structure-Function Relationships Based on Simultaneous Probability Map and Information Theory. *Society for Neuroscience 33rd Annual Meeting,* New Orleans, USA, Nov. 8-12, 2003

[46] Yamamoto T, Takahashi S, Hanakawa T, Urayama S, Aso T, Fukuyama H & Ejima Y. (2008). Neural correlates of the stereokinetic effect revealed by functional magnetic resonance imaging. *J Vis,* Vol.8, No.10, pp. 141-17, ISSN 1534-7362